Identification of F X in the Heliobacterial Reaction Center as a [4Fe-4S] Cluster with an S = 3 / 2 Ground Spin State †

ARTICLE *in* BIOCHEMISTRY · JUNE 2006

Impact Factor: 3.02 · DOI: 10.1021/bi060031s · Source: PubMed

5 AUTHORS, INCLUDING:

Mark L Heinnickel
Stanford University
20 PUBLICATIONS **214** CITATIONS
SEE PROFILE

Nina Svensen
Weill Cornell Medical College
12 PUBLICATIONS **302** CITATIONS
SEE PROFILE

Identification of F_X in the Heliobacterial Reaction Center as a [4Fe-4S] Cluster with an $S = {}^3/_2$ Ground Spin State†

Mark Heinnickel,‡ Rufat Agalarov,‡ Nina Svensen,‡,§ Carsten Krebs,*,‡,|| and John H. Golbeck*,‡,||

Department of Biochemistry and Molecular Biology and Department of Chemistry, The Pennsylvania State University, University Park, Pennsylvania 16802

Received January 6, 2006; Revised Manuscript Received March 23, 2006

ABSTRACT: Type I homodimeric reaction centers, particularly the class present in heliobacteria, are not well understood. Even though the primary amino acid sequence of PshA in *Heliobacillus mobilis* has been shown to contain an F_X binding site, a functional Fe−S cluster has not been detected by EPR spectroscopy. Recently, we reported that PshB, which contains F_A- and F_B-like Fe−S clusters, could be removed from the *Heliobacterium modesticaldum* reaction center (HbRC), resulting in 15 ms lifetime charge recombination between $P798^+$ and an unidentified electron acceptor [Heinnickel, M., Shen, G., Agalarov, R., and Golbeck, J. H. (2005) *Biochemistry 44*, 9950−9960]. We report here that when a HbRC core is incubated with sodium dithionite in the presence of light, the 15 ms charge recombination is replaced with a kinetic transient in the sub-microsecond time domain, consistent with the reduction of this electron acceptor. Concomitantly, a broad and intense EPR signal arises around $g = 5$ along with a minor set of resonances around $g = 2$ similar to the spectrum of the $[4Fe\text{-}4S]^+$ cluster in the Fe protein of *Azotobacter vinelandii* nitrogenase, which exists in two conformations having $S = {}^3/_2$ and $S = {}^1/_2$ ground spin states. The Mössbauer spectrum in the as-isolated HbRC core shows that all of the Fe is present in the form of a $[4Fe\text{-}4S]^{2+}$ cluster. After reduction with sodium dithionite in the presence of light, approximately 65% of the Fe appears in the form of a $[4Fe\text{-}4S]^+$ cluster; the remainder is in the $[4Fe\text{-}4S]^{2+}$ state. Analysis of the non-heme iron content of HbRC cores indicates an antenna size of 21.6 ± 1.1 BChl *g* molecules/P798. The evidence indicates that the HbRC contains a [4Fe-4S] cluster identified as F_X that is coordinated between the PshA homodimer; in contrast to F_X in other type I reaction centers, this [4Fe-4S] cluster exhibits an $S = {}^3/_2$ ground spin state.

Type I homodimeric reaction centers, particularly the class present in Heliobacteriaceae, are among the most poorly understood of all photosynthetic complexes. Three-dimensional X-ray crystal structures exist at atomic resolution for the purple non-sulfur bacterial reaction center (*1*, *2*) and for cyanobacterial photosystem I (PS I)[1] (*3*), and the protein backbone and cofactor arrangement is known from near-atomic resolution X-ray data for higher-plant PS I (*4*) and cyanobacterial photosystem II (*5*−*7*). In contrast, the number and identities of electron transfer cofactors as well as the number and identities of polypeptides that constitute the heliobacterial reaction center (HbRC) remain obscure.

What is known with certainty concerns the early light-induced reactions. The primary electron donor, P798, is considered to be a dimer of Bchl *g*′ (the 13^2 epimer that now appears to be a common feature of all type I RCs), and the cation is delocalized over both molecules (*8*, *9*). The primary acceptor is Chl *a* 670, an 8^1-hydroxy Chl *a* molecule. Charge separation between P798 and A_0 occurs within 25 ps of a flash, but this may represent energy transfer from the thermally populated antenna; the actual time of charge separation is estimated to be 1 or 2 ps (*10*, *11*). Forward electron transfer from A_0^- occurs in 600 ps at room temperature, and if blocked, charge recombination between $P798^+$ and A_0^- occurs in 17 ns, repopulating the triplet state of P798.

In contrast, less is known about the intermediate and tertiary electron acceptors. Membranes contain large quantities of menaquinone-9 (as well as some menaquinone-8 and menaquinone-10), but isolated HbRCs have been reported to contain as little as one molecule or less (*12*). EPR (*13*) and ENDOR (*14*) studies show a photoaccumulated signal consistent with a semiquinone radical, but optical kinetic and photovoltage experiments (*15*) have failed to confirm a

† Supported by grants to J.H.G. from the U.S. Department of Energy (DE-FG02-98ER20314) and the U.S. National Science Foundation (MCB-0117079).

* To whom correspondence should be addressed. C.K.: telephone, (814) 865-6089; fax, (814) 863-7024; e-mail, ckrebs@psu.edu. J.H.G.: telephone, (814) 865-1163; fax, (814) 863-7024; e-mail, jhg5@psu.edu.

‡ Department of Biochemistry and Molecular Biology.

§ Current address: Department of Chemistry, Technical University of Denmark, 2800 Kgs. Lyngby, Denmark.

|| Department of Chemistry.

[1] Abbreviations: PS I, photosystem I; Fe−S, iron−sulfur; EPR, electron paramagnetic resonance; HbRC, reaction center from *Heliobacterium modesticaldum*; PshA, photosynthetic reaction center protein from heliobacteria; PshB, low-molecular mass Fe−S protein bound to the HbRC; HbRC core, HbRC without the PshB protein; BChl *g*, bacteriochlorophyll *g*; *Av*, *Azotobacter vinelandii*; *Hm*, *He. modesticaldum*; SDS−PAGE, sodium dodecyl sulfate−polyacrylamide gel electrophoresis.

10.1021/bi060031s CCC: $33.50
Published on Web 05/03/2006

functional quinone intermediate. A broad and featureless optical difference spectrum in urea-treated membranes of *Heliobacillus mobilis* provides the only evidence of an F_X-like Fe−S cluster (*16*), the existence of which is nevertheless implied by a conserved FPCxGPxxGGTC motif on the PshA reaction center polypeptide (*17*). Surprisingly, the presence of F_X could not be confirmed by EPR spectroscopy in membranes of *Heliobacterium chlorum*, although a well-defined set of resonances shows the presence of F_A- and F_B-like Fe−S clusters (*18*).

We recently carried out a series of systematic experiments aimed at re-examining the issue of the participation of Fe−S clusters in the photosynthetic reaction center of *Heliobacterium modesticaldum* (*Hm*), a thermophile that grows in hot springs and volcanic soils (*19*). We showed that the intact photosynthetic reaction center of *Hm* (HbRC) could be isolated from membranes using *n*-dodecyl-β-D-maltopyranoside and partially purified on a sucrose density gradient (*20*). The low-temperature EPR spectrum of a sample that was illuminated at 20 K exhibits a rhombic spectrum, with *g* values of 2.067, 1.933, and 1.890, which is attributed to a single $[4Fe\text{-}4S]^+$ cluster. The EPR spectrum of a sample that was continuously illuminated during freezing is more complex and exhibits multiple resonances spanning *g* values from 2.04 to 1.90; these features were assigned to two $[4Fe\text{-}4S]^+$ clusters, which are dipolar coupled. The low-molecular mass protein containing the Fe−S clusters, which we termed PshB, could be dissociated from the HbRC by washing with 1.0 M NaCl and removed by ultrafiltration over a 30 kDa cutoff membrane. The resulting HbRC core, which was further purified by ion-exchange chromatography, could rebind PshB, resulting in the recovery of light-induced EPR signals of the F_A- and F_B-like Fe−S clusters (*20*).

The isolation of an intact, functional HbRC core provided an opportunity to study the electron acceptor that immediately precedes F_A and F_B. The flash-induced kinetics of the intact HbRC complex show two kinetic phases at room temperature, one with a lifetime of ca. 75 ms and the other with a lifetime of ca. 15 ms. The 75 ms component is lost when PshB is removed from the HbRC complex, and it is regained when PshB is rebound to HbRC cores (*20*). Thus, the 15 ms kinetic phase is derived from recombination of $P798^+$ with an earlier acceptor that remained unidentified, but which we proposed might be F_X. However, we were unable to measure an EPR spectrum of an Fe−S cluster after photoaccumulation of HbRC cores in the presence of sodium dithionite at pH 10.0 (see also ref *16*), conditions that should have allowed us to detect F_X^-. We suggested that this could be because the F_X cluster has exceedingly rapid relaxation properties or an unusual ground spin state; both would make detection by EPR difficult. The work presented here is directed toward obtaining unequivocal EPR and Mössbauer evidence for the presence of a [4Fe-4S] cluster in HbRC cores.

MATERIALS AND METHODS

Isolation of HbRC Cores. Cultures of *Hm* were generously provided by M. Madigan (Southern Illinois University, Carbondale, IL). Liquid cultures of *Hm* were grown anaerobically in PYE media as described in ref *19* except that 50 μmol of ^{57}Fe was added to the growth medium. Resazurin, an oxygen reporter dye, was also added to a final concentration of 0.001%. All manipulations were performed anaerobically. Plasticware and glassware were placed in the anaerobic chamber 3 h prior to use and tested with a resazurin solution to verify that any residual oxygen had been removed. Cells grown to late-exponential phase were harvested at 10000*g* and resuspended in 50 mM MOPS buffer (pH 7). Whole cells were lysed by sonication, and membranes were pelleted by centrifugation at 200000*g*. Membranes were solubilized with 1% *n*-dodecyl-β-D-maltopyranoside for 1 h, and intact membranes were removed by centrifugation at 200000*g*. Solubilized membranes were passed over a diethylaminoethyl cellulose ion-exchange column equilibrated in 50 mM MOPS (pH 7.0). The flowthrough contained the HbRC cores, which were concentrated by ultrafiltration to 15 mM Chl (1200 OD at 788 nm) and divided into three aliquots: one diluted 1500-fold and used for time-resolved optical studies and the other two used without dilution for EPR studies and Mössbauer studies. The identical sample of ^{57}Fe-containing HbRC cores was therefore used for all of the spectroscopic studies described in this paper.

Bacteriochlorophyll and Iron Analyses. The amount of bacteriochlorophyll *g* was measured in acetone using a previously published molar extinction coefficient (*21*). A 10 μL aliquot of HbRC cores was added to 990 μL of acetone; the sample was vortexed and spun at 10000*g*, and the optical density of the supernatant was measured at 762 nm. The amount of non-heme iron was measured according to a previously described protocol (*22*) with minor modifications. A 300 μL aliquot of HbRC cores was added to 300 μL of reagent A (4.5% sodium dodecyl sulfate and a 1.5% saturated solution of sodium acetate) and 300 μL of reagent B (273 mM ascorbic acid, 8.45 mM sodium meta-bisulfate, and a 6.6% saturated solution of sodium acetate), and the mixture was incubated at 37 °C for 15 min. A total of 15 μL of reagent C [36 mM 3-(2-pyridyl)-5,6-di(2-furyl)-1,2,4-triazine-5′,5″-disulfonic acid, sodium salt, also known as ferene] was added, and the optical density was measured at 593 nm. A control was prepared without adding reagent C, and the optical density was measured similarly. The difference between the sample and control represented the optical density from the iron−ferene complex. The standard curve was constructed from a freshly prepared solution of $Fe^{II}(NH_4)_2(SO_4)_2 \cdot 6H_2O$.

Time-Resolved Optical Spectroscopy. The kinetics of reduction of the primary electron donor were measured by monitoring the flash-induced absorbance change at 798 nm. The sample was placed in a 1 cm × 1 cm quartz cuvette. Actinic illumination was provided by a Nd:YAG laser (Quanta-Ray DCR-11, Spectra-Physics, Mountain View, CA) operated in the second harmonic ($\lambda = 532$ nm) with a 7 ns duration and an energy of $\sim$2 mJ/cm^2. The measuring beam was derived from a 400 W tungsten−halogen lamp (model 66057, Oriel Corp., Stratford, CT), which was passed sequentially through a $^1/_4$ m monochromator (model 82-410, Jarrell-Ash. Co., Waltham, MA) and a shutter (Uniblitz model T132, Vincent Associates, Rochester, NY). The beam was monitored using a biased Si photodiode (PIN10D, UDT Sensors, Inc., Hawthorne, CA) shielded from stray light by a narrow-band interference filter centered at 800 nm (Corion). The shutter was opened 20 ms before the onset of the laser

flash. The signal from the photodiode was amplified with an AM502 differential amplifier (Tektronix, Beaverton, OR), digitized with a DSA601 digital oscilloscope (Tektronix), and processed on a Power Macintosh computer (model 9500, Apple Computer, Cupertino, CA) that was interfaced with the digitizer via an IEEE-488 bus (PCI-GPIB, National Instruments, Austin, TX). The electronic bandwidth of the detection system was 1 MHz. Typically, 8−10 transients were averaged. Kinetic traces were analyzed by fitting the multiexponential decay using the Marquardt least-squares algorithm program in Igor Pro (Wavemetrics, Lake Oswego, OR). The samples were suspended in 50 mM MOPS (pH 7.0) to an OD of 0.8 at 788 nm.

EPR Spectroscopy. Low-temperature EPR spectroscopy was performed using an ECS-106 X-band spectrometer (Bruker Biospin, Billerica, MA) equipped with an ESR900 liquid helium cryostat and an ITC-4 temperature controller (Oxford Instruments, Billerica, MA). The HbRC cores were loaded into the EPR sample tubes along with 33 mM sodium dithionite and 100 mM glycine (pH 10.0). The samples were photoaccumulated by fitting the EPR tube with a vacuum adaptor and illuminating the sample with a 3 W Series 2000 argon ion laser (Spectra-Physics) in an outboard glass dewar under conditions that allowed the sample to be frozen slowly to 77 K. A 3-fold beam expander ensured a uniform illumination of the sample tube during freezing.

Values for the zero-field splitting parameter D were estimated using a previously described protocol (*23*). The populations of the two Kramers doublets of the $S = {}^3/_2$ ground state were estimated at g values of 4.4 and 5.4. A plot of the natural logarithm of the ratio of the peak intensities versus the inverse of the absolute temperature is fit to a straight line, the slope of which yields the energy separation, Δ, of the two Kramers doublets of the $S = {}^3/_2$ ground state.

Mössbauer Spectroscopy. Mössbauer spectra were recorded on spectrometers from WEB Research (Edina, MN) operating in the constant acceleration mode in transmission geometry. Spectra were recorded with the temperature of the sample at 4.2 K maintained with a liquid helium cryostat. For low-field spectra, the sample was kept inside a SVT-400 dewar (Janis, Wilmington, MA) and a magnetic field of 40 mT was applied parallel to the γ-beam. For high-field spectra, the sample was kept inside a 12SVT dewar (Janis), which houses a superconducting magnet that allows for application of variable fields between 0 and 8 T parallel to the γ-beam. The isomer shifts quoted are relative to the centroid of the spectrum of a metallic foil of Fe at room temperature. Data analysis was performed using WMOSS from WEB Research. Some of the simulations are based on the spin Hamiltonian formalism, given by the following equations, in which the first three terms describe the electron Zeeman effect and zero-field splitting of the $S = {}^3/_2$ ground state, the fourth term represents the interaction between the electric field gradient and the nuclear quadrupole moment, the fifth term describes the magnetic hyperfine interactions of the electronic spin with the ^{57}Fe nuclei, and the last term represents the nuclear Zeeman interaction. Simulations for both spectroscopically distinct sites (diferrous pair and mixed-valent pair) of the $[4Fe\text{-}4S]^+$ cluster were carried out with respect to the electronic spin of the $S = {}^3/_2$ ground state.

$$H = \beta \mathbf{S}\cdot\mathbf{g}\cdot\mathbf{B} + D\left[S_z^2 - \frac{S(S+1)}{3}\right] + E(S_x^2 - S_y^2) + \sum_{i=1}^{2}\frac{eQV_{zz,i}}{4}\left[I_{z,i}^2 - \frac{I_i(I_i+1)}{3} + \frac{\eta}{3}(I_{x,i}^2 - I_{y,i}^2)\right] + \sum_{i=1}^{2}\mathbf{S}\cdot\mathbf{A}_i\cdot\mathbf{I}_i - \sum_{i=1}^{2} g_n\beta_n\mathbf{B}\cdot\mathbf{I}_i$$

RESULTS

Reduction of Acceptor X in HbRC Cores by Photoaccumulation. HbRC cores were prepared by stripping PshB from HbRC complexes with 1 M KCl followed by ion-exchange chromatography (*20*). As shown in Figure 1 (top), the flash-induced absorption change at 798 nm in the resulting HbRC core decays monotonically with a lifetime of 16 ms. The total absence of the ca. 75 ms decay component indicates that the PshB protein, which contains the F_A and F_B clusters, has been completely removed. We tentatively denote the electron acceptor responsible for the 16 ms kinetic transient in purified HbRC cores as component X. Prolonged exposure to air does not alter the amplitude or kinetics of the flash-induced transient, indicating that unlike F_A and F_B, X is stable to dioxygen. Because the addition of 2 mM sodium dithionite at pH 10.0 did not alter the amplitude or kinetics of the 16 ms component on a single-turnover flash, X cannot be reduced chemically. However, the application of successive laser flashes to the sample resulted in the progressive loss of amplitude of the 16 ms decay component such that 50% of the absorbance change was lost after nine flashes and 85% of the absorbance change was lost after 90 flashes (data not shown). A continuous beam of white light produced the same effect; as shown in Figure 1 (bottom), more than 95% of the amplitude of the 15 ms decay component was lost after illumination for 1 min. The missing amplitude represents either rapid charge separation followed by recombination between P798 and an electron acceptor that precedes X or a damaged HbRC core. When the pH was lowered to 7.0 by addition of aerobic buffer, the 16 ms phase returned (data not shown), indicating that X is reduced rather than damaged. Under both illumination protocols, a kinetic transient with a lifetime of 23 μs becomes visible (Figure 1, bottom), the magnitude of which does not depend on the loss of amplitude of the 16 ms decay phase. Because its amplitude is a function of the laser flash intensity (data not shown), this component is tentatively assigned to the decay of an antenna chlorophyll triplet.

As-Isolated HbRC Cores Contain a $[4Fe\text{-}4S]^{2+}$ Cluster. To determine whether X is an Fe−S cluster, we studied as-isolated ^{57}Fe-enriched HbRC cores by Mössbauer spectroscopy. The spectrum, which was recorded at 4.2 K in an externally applied 40 mT magnetic field oriented parallel to the γ-beam, is shown in Figure 2 (top) as hash marks. It is a sharp (line width, $\Gamma_{left} = 0.25$ mm/s and $\Gamma_{right} = 0.29$ mm/s) quadrupole doublet with parameters typical of $[4Fe\text{-}4S]^{2+}$ clusters: isomer shift $\delta = 0.45 \pm 0.02$ mm/s and quadrupole splitting parameter $\Delta E_Q = 1.07 \pm 0.02$ mm/s (Figure 2, top, solid line). This quadrupole doublet accounts for 97 ± 3% of the total intensity of the spectrum. The spectrum of this sample recorded in an external 8 T magnetic field oriented parallel to the γ-beam is shown in Figure 2

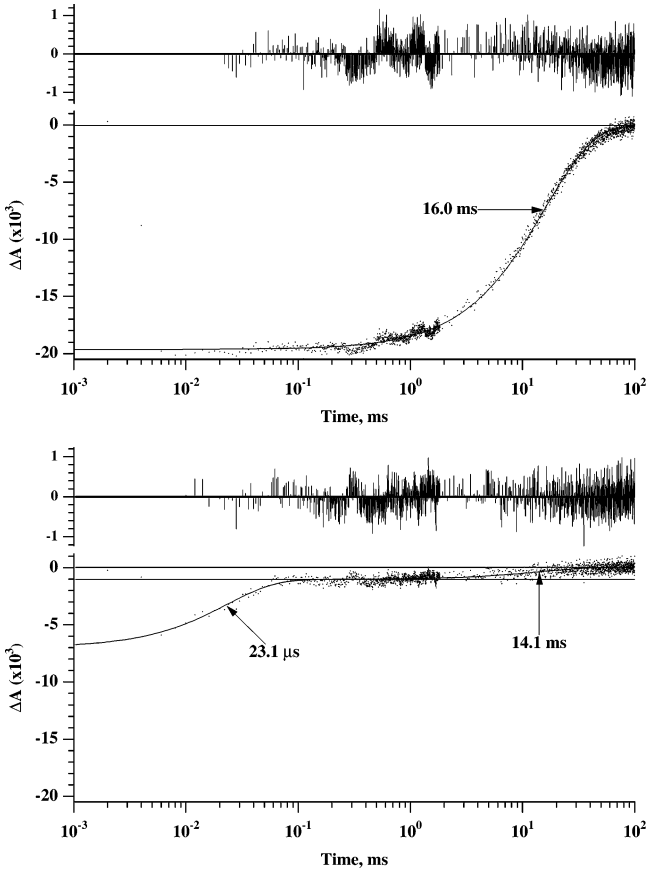

FIGURE 1: Flash-induced absorption changes of $P798^+$ in HbRC cores in the presence of 1 mM ascorbate and 50 mM MOPS (pH 7.0) (top) and 2 mM dithionite, 100 mM glycine (pH 10.0), and illumination for 1 min (bottom). Both samples had an optical transmittance at 788 nm of 0.80 OD. The plots depict an average of 16 traces acquired at 10 s intervals. Time is plotted on a logarithmic scale in which a deviation from the horizontal represents a kinetic phase. The computer-generated exponential fit is shown as a solid line. Results of the exponential fits are displayed as fit curves, where each individual component is plotted with a vertical offset relative to the next component (with a longer lifetime) or the baseline, the offset being equal to the amplitude of the latter component. The relative contributions of each kinetic phase can be judged by the intersection of the fit line with the abscissa. The residual of the fit is depicted above the main trace.

(bottom). By using the Mössbauer parameters obtained from the 40 mT spectrum, it is possible to determine the effective magnetic field experienced by the ^{57}Fe nuclei to be 8 T, i.e., the magnitude of the effective magnetic field equals that of the externally applied magnetic field. This means that the internal magnetic field is zero and that the Fe sites have a diamagnetic ($S = 0$) ground state. A simulation using the spin Hamiltonian formalism assuming diamagnetism, values of δ and ΔE_Q determined from the 40 mT spectrum, and an asymmetry parameter (η) 0.4 ± 0.1 is shown as solid line overlaid with the experimental data. Without exception, $[4Fe\text{-}4S]^{2+}$ clusters have a diamagnetic ground state, and consequently, the 8 T spectrum is in full conformity with the presence a $[4Fe\text{-}4S]^{2+}$ cluster in as-isolated HbRC cores. Other Fe species, such as different Fe−S cluster types or adventitiously bound Fe, represent not more than 3% of the total Fe contained in the sample.

Cytochrome Content of HbRC Cores. The type I homodimeric reaction center from *Chlorobium limicola* contains a bound cytochrome c_{553} (*24*). Like other prokaryotic

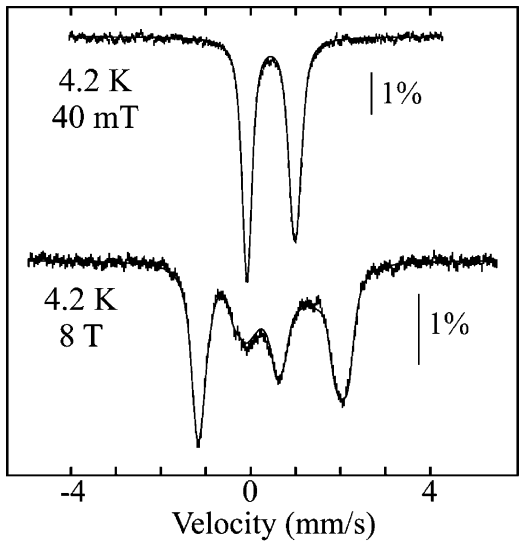

FIGURE 2: Mössbauer spectra of ^{57}Fe-enriched HbRC cores recorded at 4.2 K in externally applied magnetic fields of 40 mT (top) and 8 T (bottom). The orientation of the magnetic field is parallel to the γ-beam. The experimental spectra are shown as hash marks. The solid line overlaid with the 40 mT spectrum is a quadrupole doublet with the following parameters: $\delta = 0.45$ mm/s, $\Delta E_Q = 1.07$ mm/s, $\Gamma_{left} = 0.25$ mm/s, and $\Gamma_{right} = 0.29$ mm/s. The solid line overlaid with the 8 T spectrum is a spin Hamiltonian simulation, using the above values for δ and ΔE_Q and an η of 0.4, and assuming diamagnetism.

cytochromes, the axial ligands are a His and a Met. The related cytochrome c_{551} from *Pseudomonas aeruginosa*, which also has a His/Met-ligated heme, has in its low-spin ferrous form Mössbauer parameters ($\delta = 0.45$ mm/s and $\Delta E_Q = 1.29$ mm/s) which are almost identical to those observed for HbRC cores (see above) (*25*). Moreover, low-spin ferrous heme centers have a diamagnetic ground state, and therefore, the Mössbauer spectroscopic features associated with the HbRC do not rule out the presence of a His/Met-ligated low-spin ferrous heme. To resolve this issue, we have studied samples of HbRC cores using biophysical methods that are capable of detecting the presence of a heme-containing cofactor. *c*-Type cytochromes have midpoint potentials of approximately 150 mV and can be oxidized to the EPR-active ferric form. Oxidized *P. aeruginosa* cytochrome c_{551}, for example, contains a low-spin ferric heme, which exhibits EPR resonances with *g* values of 3.2 and 2.05 (*26*). HbRC complexes and HbRC cores that were oxidized with ammonium persulfate in the presence of air showed no evidence of either a high-spin or a low-spin cytochrome in either sample by EPR spectroscopy (data not shown). Heme cofactors display an intense feature in the visible region; the so-called Soret band is located in the 500−555 nm range for *c*-type cytochromes (*27*), a region in which BChl *g* minimally absorbs. We failed to find any evidence of the presence of a *c*-type cytochrome in HbRC cores by optical spectroscopy. Heme proteins can be identified by staining with benzidine dyes (*28*). We separated the polypeptides in the HbRC cores by SDS−PAGE followed by staining with 3,3′,5,5′-tetramethylbenzidine and found no evidence of a *c*-type cytochrome. We conclude that a bound *c*-type cytochrome is absent in our preparations of HbRC cores from *Hm*. Thus, the Mössbauer spectra of as-isolated HbRC cores emanate from $[4Fe\text{-}4S]^{2+}$ clusters and not from a low-spin ferrous *c*-type cytochrome.

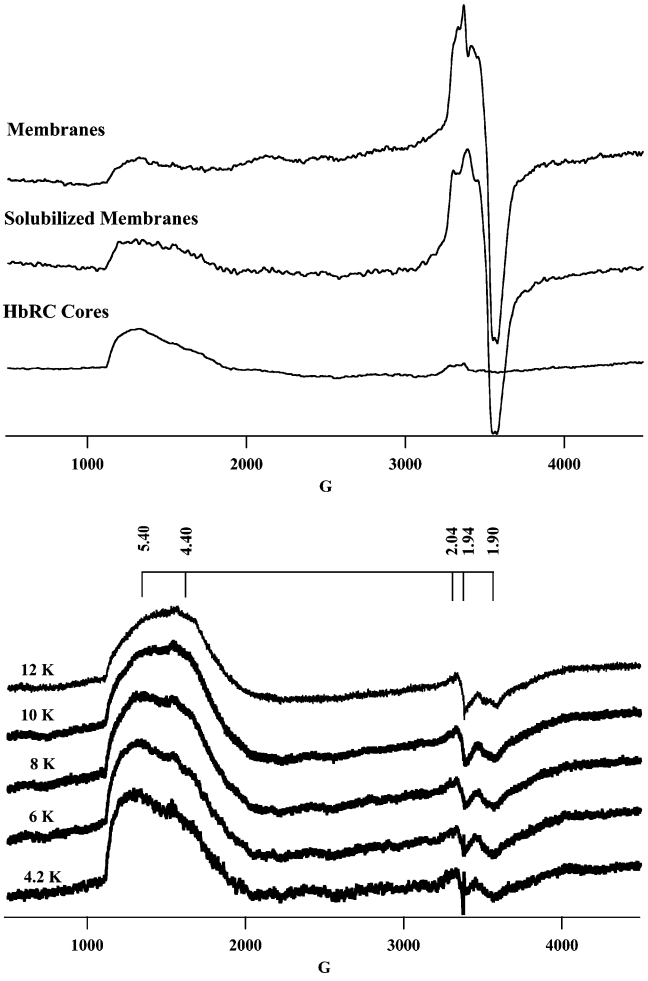

FIGURE 3: EPR spectra of photoaccumulated membranes, detergent-solubilized membranes, and HbRC cores measured at 4.2 K (top). The spectra represent 10 averages of 1000 total data points. EPR spectra of photoaccumulated HbRC cores measured at temperatures from 4.2 to 12 K (bottom). The spectra represent four averages of 8000 total data points. The effective *g* values of the resonances are depicted. EPR conditions: microwave power, 126 mW; microwave frequency, 9.47 GHz; receiver gain, 2×10^4; modulation amplitude, 10 G at 100 kHz.

Non-Heme Iron and Bacteriochlorophyll g Content of HbRC Cores. Iron and BChl *g* concentrations were measured on six HbRC core samples ranging from 1.0 to 15 mM Bchl *g*. Five identical samples were analyzed at each bacteriochlorophyll concentration. In a total of 30 samples, the BChl *g*/Fe ratio was found to be 5.49 ± 0.27 (mean ± standard deviation). Our Mössbauer spectroscopic results indicate that 97% of the Fe in as-isolated HbRC cores is in the form of $[4Fe\text{-}4S]^{2+}$ clusters, which translates to a BChl *g*/$[4Fe\text{-}4S]^{2+}$ ratio of 21.6 ± 1.1.

Reduced X Is a [4Fe-4S]$^+$ Cluster with an $S = {}^3/_2$ Ground State. Highly concentrated HbRC cores were subject to a similar photoaccumulation protocol (described in Materials and Methods) and examined by low-temperature EPR spectroscopy. As shown in Figure 3 (top), resonances from F_A and F_B are present around 3500 G in membranes and detergent-solubilized membranes, but as expected, they are missing in HbRC cores. In all three samples, a broad, intense signal is present between 1200 and 2000 G. At 4.2 K, the low-field resonance shows two distinctive features: a peak at $g = 5.4$ and a shoulder at $g = 4.4$ (Figure 3, bottom). As the temperature is increased to 12 K, the $g = 5.4$ peak decreases in intensity while the $g = 4.4$ shoulder increases in intensity. These resonances can be assigned to a $[4Fe\text{-}4S]^+$ cluster with an $S = {}^3/_2$ ground spin state. The temperature dependence suggests that the $g = 5.4$ signal emanates from the ground Kramers doublet, whereas the $g = 4.4$ feature is associated with the excited Kramers doublet of the $S = {}^3/_2$ spin manifold. We estimate the energy difference, Δ, between the two Kramers doublets from the relative intensity of the two signals to be approximately 3 cm^{-1} (see the Supporting Information). Because Δ is related to the zero-field splitting parameters *D* and *E*/*D* (eq 1), we estimate $|D| \approx 1.5$ cm^{-1}.

$$\Delta = 2D\sqrt{1 + 3(E/D)^2} \quad (1)$$

The *g* values of approximately 5.4 and 4.4 are expected for an $S = {}^3/_2$ spin system exhibiting a rhombicity, *E*/*D*, of approximately 0.2 (see also the Mössbauer studies below). Assuming $D < 0$, such a system exhibits *g* values of 5.8, 1.3, and 1.0 for the ground doublet and 5.0, 2.7, and 1.8 for the excited doublet. The fact that *g* values are not well resolved suggests significant heterogeneity of the sample, which could result in a distribution of *E*/*D* values and broadened spectra. Rhombograms are derived for the case in which $D \gg g\beta B$. However, on the basis of the temperature dependence of the signal, we estimate *D* to be small. We have also considered the possibility that the broadness of the EPR features is caused by mixing of the ZFS interaction and the Zeeman interaction. A simulation of the EPR spectrum based on diagonalization of the spin Hamiltonian matrix (*29*−*31*) and assuming discrete values for *E*/*D* of 0.2 and for *D* of −1.5 cm^{-1} yields a spectrum similar to that predicted by *g* values obtained from a rhombograms for which $D \gg g\beta B$ (not shown). This suggests that the observed EPR features are not due to the small ZFS parameters but rather result as a consequence of a distribution of ZFS parameters.

The feature in the $g = 2$ region is characteristic of a $[4Fe\text{-}4S]^+$ cluster with an $S = {}^1/_2$ ground spin state. One possibility is that this signal emanates from a small amount of PshB (containing reduced F_A and F_B) that has not been removed from the HbRC complex. In support of this proposal, *g* values of 2.04 and 1.90, as well as the spin relaxation properties, as inferred from the temperature dependence of the resonances (not shown), are similar to those of reduced F_A/F_B in HbRC complexes (*20*). A second possibility is that reduced X may exist in different conformations with $S = {}^3/_2$ and $S = {}^1/_2$ ground states. In the case of the Fe protein of *Av* nitrogenase, the addition of 50% ethylene glycol favors the $S = {}^1/_2$ ground state, whereas the addition of 0.4 M urea favors the $S = {}^3/_2$ ground state (*32*). In HbRC cores, however, no alteration in the relative populations of the $g = 5.4/4.4$ and $g = 1.94$ resonances was found in HbRC cores after addition of ethylene glycol or urea. The origin of the $g \sim 2$ signals, therefore, remains unresolved, although the integrated intensity of the resonances corresponds to less than 2% of the amount of F_A and F_B present in intact HbRC complexes.

An identical sample of photoaccumulated HbRC cores was characterized further by Mössbauer spectroscopy (Figure 4). The 4.2 K/40 mT Mössbauer spectrum (left panel, top spectrum) exhibits, in addition to two sharp lines, a broad and featureless absorption extending from −1.5 to 2.0 mm/

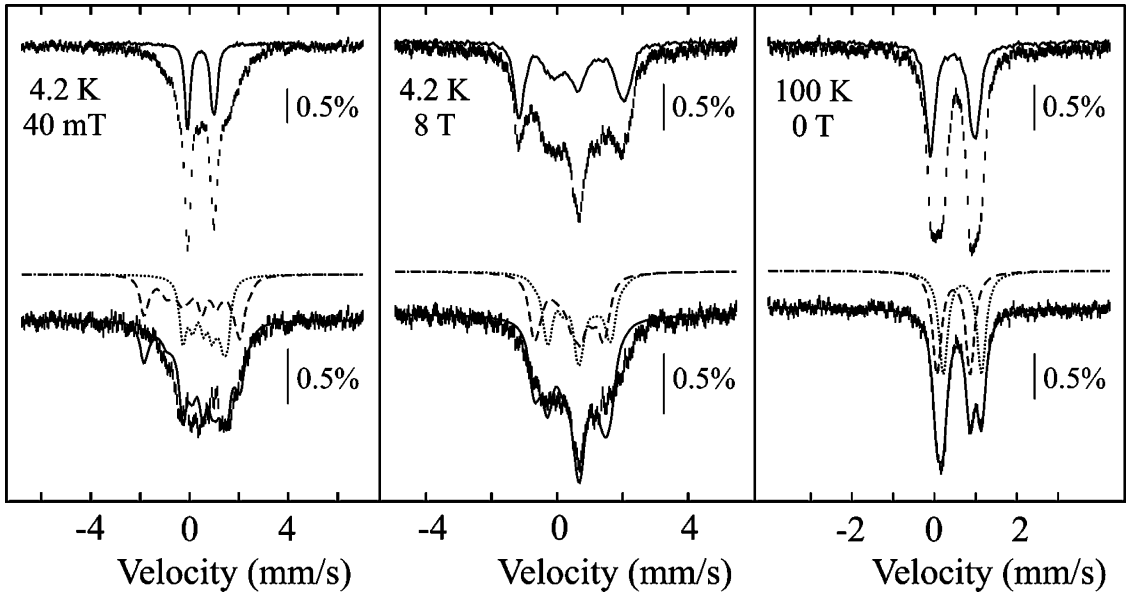

FIGURE 4: Mössbauer spectra of ^{57}Fe-enriched photoaccumulated HbRC cores recorded at 4.2 K in a 40 mT magnetic field (left panel), 4.2 K in an 8 T magnetic field (middle panel), and 100 K without an applied field (right panel). The experimental spectra are shown on top as hash marks. The solid lines are spectra of as-isolated HbRC cores recorded under the same experimental conditions and scaled to 35% of the intensity of the respective hash-marked spectrum. Removal of the contribution of the $[4Fe\text{-}4S]^{2+}$ clusters of nonreduced HbRC results in the reference spectra of reduced X, the $[4Fe\text{-}4S]^{+}$ cluster with an $S = {}^3/_2$ ground spin state (hash-marked spectra at the bottom of each panel). The solid lines overlaid with the reference spectra are simulations of the $[4Fe\text{-}4S]^{+}$ cluster described in the text. Individual contributions from the diferrous and mixed-valent site of the cluster are shown as dotted and dashed lines, respectively. Simulations of the 4.2 K data were generated by using the spin Hamiltonian formalism in the slow relaxation limit with the following parameters: $S = {}^3/_2$, $D_{3/2} = -1.5$ cm^{-1}, $(E/D)_{3/2} = 0.2$, $g = 2.0$, $\delta(1) = 0.46$ mm/s, $\Delta E_Q(1) = -0.80$ mm/s, $\eta(1) = 0.8$, $A_{iso}(1)/g_N\beta_N = -8.6$ T, and $\delta(2) = 0.68$ mm/s, and $\Delta E_Q(2) = -0.93$ mm/s, $\eta(2) = -10$, and $A_{iso}(2)/g_N\beta_N = -2.9$ T. The 100 K data were simulated with two quadrupole doublets with the following parameters: $\delta(1) = 0.46$ mm/s and $\Delta E_Q(1) = 0.80$ mm/s (dashed line) and $\delta(2) = 0.68$ mm/s and $\Delta E_Q(2) = 0.93$ mm/s (dotted line).

s. Comparison of this spectrum to the 4.2 K/40 mT spectrum of as-isolated HbRC cores (solid line) reveals that the two sharp lines emanate from a nonreduced $[4Fe\text{-}4S]^{2+}$ cluster. Analysis of the spectrum reveals that $35 \pm 5\%$ of the total intensity can be attributed to $[4Fe\text{-}4S]^{2+}$ clusters. (Unlike the optical studies depicted in Figure 1, the EPR and Mössbauer studies require much higher sample concentrations, which preclude quantitative photoreduction of the sample.) Removal of its spectral contribution results in the reference spectrum of reduced X (Figure 4, bottom left), which is broad and featureless. The broadening is caused by the magnetic hyperfine interactions between the electronic spin and the ^{57}Fe nuclei. Detection of magnetically split Mössbauer spectra in a small (40 mT) magnetic field is typical of Fe centers having a half-integer electron spin ground state and electronic fluctuation rates slower than the ^{57}Fe nuclear Larmor frequency. We have considered the possibility that the broad and featureless spectrum is a consequence of the intermediate relaxation regime and recorded the spectrum of this sample at 2 K in a 40 mT magnetic field. Since this spectrum (data not shown) is essentially identical to that recorded at 4.2 K, we conclude that the broad features are not a consequence of intermediate relaxation.

At higher temperatures and without an applied magnetic field, the Mössbauer features of $[4Fe\text{-}4S]^{+}$ clusters typically collapse into quadrupole doublets. We have recorded the 100 K/zero-field spectrum of photoaccumulated HbRC cores, which is shown in Figure 4, top right, as hash marks. Plotted as a solid line is the 100 K/zero-field spectrum of as-isolated HbRC cores scaled to 35% of the total intensity. Removal of this contribution results in the 100 K/zero-field reference spectrum of reduced X (Figure 4, bottom right). This spectrum exhibits a broad line at 0.14 mm/s and two sharp, well-resolved lines at 0.86 and 1.14 mm/s. Importantly, the latter two lines have similar intensity and width, suggesting the presence of two quadrupole doublets that are equal in intensity. The low-energy lines of the two quadrupole doublets overlap and give rise to the more intense peak at 0.14 mm/s. We have analyzed this spectrum with two symmetrical ($\Gamma_{left} = \Gamma_{right}$) quadrupole doublets equal in intensity and width. We obtain two fits of equal quality, depending on how the four lines are paired. The first fit involves combining the inner lines to one quadrupole doublet and the outer lines to the other quadrupole doublet, yielding the following parameters: $\delta(1) = 0.54$ mm/s, $|\Delta E_Q(1)| = 0.65$ mm/s, $\delta(2) = 0.60$ mm/s, and $|\Delta E_Q(2)| = 1.08$ mm/s. For the second fit, we pair lines one and three to the first quadrupole doublet and lines two and four to the second quadrupole doublet: $\delta(1) = 0.46$ mm/s, $|\Delta E_Q(1)| = 0.80$ mm/s, $\delta(2) = 0.68$ mm/s, and $|\Delta E_Q(2)| = 0.93$ mm/s. This simulation is shown as a solid line in Figure 4 (bottom right), and the individual contribution of the first (second) quadrupole doublet is shown as a dashed (dotted) line for clarity.

Of these two possibilities, we favor the second for the following reason. The fact that we observe two at least partially resolved quadrupole doublets of equal intensity suggests that the spectrum of the $[4Fe\text{-}4S]^{+}$ cluster is comprised of two distinct pairs of Fe ions. The Mössbauer parameters of the first pair [$\delta(1) = 0.46$ mm/s and $|\Delta E_Q(1)| = 0.80$ mm/s] are typical of a valence-delocalized $Fe^{2.5}-Fe^{2.5}$ unit. The other diiron pair then has to be a diferrous pair. The Mössbauer parameters of the second pair [$\delta(2) = 0.68$ mm/s

and $|\Delta E_Q(2)| = 0.93$ mm/s], in particular the high isomer shift, support this assignment. For example, the isomer shift of the Fe sites of the all-ferrous $[4Fe\text{-}4S]^0$ cluster from the *Av* Fe protein is 0.68 mm/s (at 4.2 K) (*33*), in good agreement with the isomer shift for the quadrupole doublet assigned to the diferrous pair of the $[4Fe\text{-}4S]^+$ cluster.

To further study the electronic structure of the $[4Fe\text{-}4S]^+$ cluster, we recorded the 4.2 K/8 T Mössbauer spectrum of the photoaccumulated HbRC cores (Figure 4, top middle, hash marks). Again, the 4.2 K/8 T spectrum of nonreduced X, scaled to 35% of the total intensity of the hash-marked spectrum, is overlaid as a solid line. Removal of this component yields the 4.2 K/8 T reference spectrum of reduced X (Figure 4, bottom middle, hash marks), which is broad and featureless. Importantly, the overall splitting of this spectrum is similar to that of the 4.2 K/40 mT spectrum (Figure 4, bottom left). The 4.2 K reference spectra can be simulated using the spin Hamiltonian formalism in the slow relaxation limit with an $S = {}^3/_2$ electronic spin with zero-field splitting (ZFS) parameters estimated from the analysis of the EPR spectra: $D = -1.5$ cm^{-1} and $E/D = 0.2$. Furthermore, we used the isomer shifts and quadrupole splitting parameters determined from the 100 K/zero-field spectrum. The **A** tensors were assumed to be isotropic, to reduce the number of variables. The solid lines overlaid with the reference spectra are simulations using the following parameters: $S = {}^3/_2$, $D_{3/2} = -1.5$ cm^{-1}, $(E/D)_{3/2} = 0.2$, $g = 2.0$, $\delta(1) = 0.46$ mm/s, $\Delta E_Q(1) = -0.80$ mm/s, $\eta(1) = 0.8$, $A_{iso}(1)/g_N\beta_N = -8.6$ T, and $\delta(2) = 0.68$ mm/s, and $\Delta E_Q(2) = -0.93$ mm/s, $\eta(2) = -10$, and $A_{iso}(2)/g_N\beta_N = -2.9$ T. The individual components of the diferrous (site 2) and mixed-valent pair (site 1) are shown as dashed and dotted lines, respectively. These parameters are not uniquely determined due to the lack of spectral resolution and the large number of variables. For example, a fit in which the larger **A** tensor component is associated with the mixed-valent sites $[A_{iso}(1)/g_N\beta_N = -3.9$ T] and the smaller **A** tensor component is associated with the diferrous sites $[A_{iso}(2)/g_N\beta_N = -9.2$ T] results in simulations that are similar in quality and cannot be ruled out. However, the overall shape and splitting of the two 4.2 K reference spectra requires the **A** tensor components to be approximately -8 and -3 T. The **A** tensors determined are those with respect to the total electronic spin of the $S = {}^3/_2$ ground state. They are related to the intrinsic **a** tensors of the *i*th iron site, $\mathbf{a}_i$, by the following equation, in which c_{ij} is the vector coupling coefficient for the *i*th Fe site and *j*th spin state.

$$\mathbf{A}_{ij} = c_{ij} \cdot \mathbf{a}_i \qquad (2)$$

Theoretical analysis of hyperfine coupling tensors in Fe−S clusters allowed Mouesca et al. (*34*) to estimate typical values for the intrinsic **a** tensors of the mixed-valent pair and the diferrous pair of $[4Fe\text{-}4S]^+$ clusters with either $S = {}^1/_2$ or $S = {}^3/_2$ ground states as $a/g_N\beta_N = -17.5$ T. Since the experimentally observed $A/g_N\beta_N$ values span an approximate range from -3 to -8 T, the spin coupling coefficients of all four Fe sites are small and positive. By adopting a spin coupling scheme, in which we couple the spin of the diferrous pair, $S_{diferrous}$, to the spin of the mixed-valent pair, $S_{mixed-valent}$, to yield the total spin, *S*, we have calculated the spin projection coefficients for all 15 states with an $S = {}^3/_2$ ground state. Several of the states have spin coupling coefficients that are in accordance with the parameters deduced from our Mössbauer analysis. As can be seen from Table S1 (see the Supporting Information), there are $S = {}^3/_2$ states that have positive spin coupling coefficients for *all four* Fe sites. Given that the spin coupling coefficients are calculated for pure spin states, i.e., without considering mixing with other spin states, and that the spin coupling coefficients cannot be determined accurately experimentally, we can only conclude that the Mössbauer spectroscopic results are fully consistent with the description of reduced X as a $[4Fe\text{-}4S]^+$ cluster with an $S = {}^3/_2$ spin state.

DISCUSSION

Assignment of the [4Fe-4S] Cluster in HbRC Cores as F_X. F_X is defined as the interpolypeptide [4Fe-4S] cluster ligated to the PsaA−PsaB heterodimer of PS I of plants, algae, and cyanobacteria and to the PscA−PscA homodimer of the reaction center of green sulfur bacteria. It functions as the immediate electron donor to the F_A and F_B clusters, which are universally located in all type I reaction centers (*20*, *35*). Using a combination of biophysical techniques, we have studied *Hm* HbRC cores from which the PshB protein has been removed by treatment with 1 M KCl. Mössbauer spectroscopy reveals that 97 ± 3% of the total Fe associated with HbRC cores is in the form of a $[4Fe\text{-}4S]^{2+}$ cluster. We have demonstrated by a combination of time-resolved optical, EPR, and Mössbauer spectroscopies that the [4Fe-4S] cluster in HbRC cores can be reduced by illumination of the sample in the presence of dithionite. The cluster to protein stoichiometry can be deduced from the amino acid sequence of the PshA protein of the closely related organism *H. mobilis*, which shows a conserved F_X binding motif (FPCxGPxxG-GTC) that contains the two cysteine residues that coordinate the interpolypeptide [4Fe-4S] cluster (*17*). Because only one such F_X binding site exists per PshA dimer, we conclude that a single [4Fe-4S] cluster is present and that it represents F_X. All known classes of type I reaction centers, heterodimeric and homodimeric, therefore contain an F_X interpolypeptide [4Fe-4S] cluster. It should be noted that this [4Fe-4S] cluster is likely the origin of the time-resolved optical difference spectrum around 430 nm reported by Kleinherenbrink et al. (*16*) in urea-treated reaction centers from *H. mobilis*.

Reduced F_X in HbRC Cores Has an $S = {}^3/_2$ Ground Spin State. In PS I of cyanobacteria and plants and in the photosynthetic reaction center from *Chlorobium*, reduced F_X is a $[4Fe\text{-}4S]^+$ cluster with an $S = {}^1/_2$ ground spin state and is observed as a set of rhombic resonances around $g = 2$ (*35*). In contrast, reduced F_X of the HbRC from *Hm* has an $S = {}^3/_2$ ground state at low temperatures. The difficulty in observing resonances from $[4Fe\text{-}4S]^+$ clusters with an $S = {}^3/_2$ ground spin state is most likely the reason that F_X in heliobacteria had not been detected by EPR. $[4Fe\text{-}4S]^+$ clusters with an $S = {}^3/_2$ ground state typically exhibit temperature-dependent resonances in the range of $g \approx 4-6$, which emanate from the two Kramers doublets of the $S = {}^3/_2$ ground state (*23*, *32*, *36*−*38*). The absolute magnitude of the *D* value of approximately 1.5 cm^{-1} for *Hm* F_X is similar to *D* values of other $[4Fe\text{-}4S]^+$ clusters with $S = {}^3/_2$ ground states, which range from ≈0.7 to ≈4 cm^{-1} (*23*, *32*, *37*, *38*). The Mössbauer spectroscopic features of F_X in *Hm* are

similar to those of the [4Fe-4S]$^+$ cluster observed in the urea-treated Fe protein from *Av* nitrogenase (*32*). Both clusters exhibit magnetically split spectra at 4.2 K in the external magnetic field. The splitting is comparably small in both weak (40 mT) and strong (8 T) external fields, suggesting that the spin projection factors are small and positive. At higher temperatures, the magnetically split spectra collapse into quadrupole doublets. For *Hm* F_X, we observed two partially resolved quadrupole doublets equal in intensity, with parameters typical of a mixed-valent pair and a diferrous pair. In contrast, the 50 K/zero-field spectrum of the *Av* Fe protein yields one broad quadrupole doublet (*32*).

It has been found that [4Fe-4S]$^+$ clusters with $S = {}^3/_2$ ground states may also exist in another conformation, which exhibits an $S = {}^1/_2$ ground state. For example, the relative proportions of the $S = {}^1/_2$ and $S = {}^3/_2$ forms of the *Av* Fe protein depend on the solution properties. Addition of 50% ethylene glycol favors the $S = {}^1/_2$ ground state, whereas the addition of 0.4 M urea favors the $S = {}^3/_2$ ground state (*32*). On the basis of the X-ray structure of the *Av* Fe protein, which shows that the [4Fe-4S] cluster is accessible to solvent (*39*), Johnson and co-workers suggested that the presence of either glycerol or urea may induce slightly different conformations of the [4Fe-4S]$^+$ cluster with different spin ground states (*23*, *40*). The fact that addition of glycerol or urea does not perturb the cluster may indicate that F_X of HbRC is not solvent accessible. This is consistent with the finding that this [4Fe-4S] cluster is also stable to dioxygen.

Antenna Size of Bchl g in HbRC Complexes. Because the non-heme iron in a HbRC core is located entirely within a [4Fe-4S] cluster that has been identified as F_X and because one F_X binding site exits per P798, the non-heme iron content can be used as a reliable metric for quantifying the number of antenna BChl *g* molecules associated with each reaction center. Our HbRC cores have been shown to contain 21.6 $\pm$ 1.1 BChl *g* molecules/P798. This value is an upper limit; any denaturation of F_X in the course of sample isolation would have led to a higher rather than lower Bchl *g*/P798 ratio. In previous work, Nuijs et al. (*41*) assumed the in vivo extinction coefficients of Bchl *g* in the absorption maximum at 788 nm and that of the bleaching of P798 at 799 nm are equivalent and estimated the antenna size in membrane fragments of *H. chlorum* to be 30 BChl *g* molecules/P798. Kobayashi et al. (*42*) arrived at a Bchl *g*/Bchl *g*′ ratio of 14.1 in reaction centers from *H. chlorum*. Assuming two Bchl *g*′ molecules per P798, this corresponds to 28.2 Bchl *g*′ molecules/P798. Kleinherenbrink et al. (*16*) assumed the extinction coefficients for the primary donor, P800, and the antenna BChl *g* are equal ($\Delta\epsilon = 100$ mM^{-1} cm^{-1}) and estimated 24 BChl *g* molecules/P800 in urea-treated reaction centers from *H. mobilis*. These values are in reasonable agreement with our value of 21.6 $\pm$ 1.1 BChl *g* molecules/P798 in HbRC cores from *H. modesticaldum*. The consensus opinion is that HbRC complexes have a small antenna complement, which is in contrast to 96 Chl *a* molecules/P700 in cyanobacterial PS I (*3*). The small antenna size is also consistent with our qualitative observation (*20*) that considerably higher light intensities are required to saturate the EPR resonances of F_A and F_B in HbRC complexes than in cyanobacterial PS I.

ACKNOWLEDGMENT

We thank Prof. Squire Booker for technical assistance.

SUPPORTING INFORMATION AVAILABLE

Spin coupling coefficients for $S = {}^3/_2$ states with positive spin coupling coefficients for all four Fe sites of the [4Fe-4S]$^+$ cluster (Table S1) and a plot of the natural logarithm of the ratio of the amplitudes at $g = 4.4$ and 5.4 versus the inverse of the absolute temperature (Figure S1). This material is available free of charge via the Internet at http://pubs.acs.org.

REFERENCES

1. Deisenhofer, J., Epp, O., Sinning, I., and Michel, H. (1995) Crystallographic refinement at 2.3 Å resolution and refined model of the photosynthetic reaction centre from *Rhodopseudomonas viridis*, *J. Mol. Biol. 246*, 429−457.
2. Deisenhofer, J., Epp, O., Miki, K., Huber, R., and Michel, H. (1984) X-ray structure analysis of a membrane protein complex. Electron density map at 3 Å resolution and a model of the chromophores of the photosynthetic reaction center from *Rhodopseudomonas viridis*, *J. Mol. Biol. 180*, 385−398.
3. Jordan, P., Fromme, P., Witt, H. T., Klukas, O., Saenger, W., and Krauss, N. (2001) Three-dimensional structure of cyanobacterial photosystem I at 2.5 Å resolution, *Nature 411*, 909−917.
4. Ben-Shem, A., Frolow, F., and Nelson, N. (2003) Crystal structure of plant photosystem I, *Nature 426*, 630−635.
5. Kamiya, N., and Shen, J. R. (2003) Crystal structure of oxygen-evolving photosystem II from *Thermosynechococcus vulcanus* at 3.7 Å resolution, *Proc. Natl. Acad. Sci. U.S.A. 100*, 98−103.
6. Zouni, A., Witt, H. T., Kern, J., Fromme, P., Krauss, N., Saenger, W., and Orth, P. (2001) Crystal structure of photosystem II from *Synechococcus elongatus* at 3.8 Å resolution, *Nature 409*, 739−743.
7. Ferreira, K. N., Iverson, T. M., Maghlaoui, K., Barber, J., and Iwata, S. (2004) Architecture of the photosynthetic oxygen-evolving center, *Science 303*, 1831−1838.
8. Noguchi, T., Fukami, Y., Oh-Oka, H., and Inoue, Y. (1997) Fourier transform infrared study on the primary donor P798 of *Heliobacterium modesticaldum*: Cysteine S-H coupled to P798 and molecular interactions of carbonyl groups, *Biochemistry 36*, 12329−12336.
9. Prince, R. C., Gest, H., and Blankenship, R. E. (1985) Thermodynamic properties of the photochemical reaction center of *Heliobacerium chlorum*, *FEBS Lett. 182*, 345−349.
10. Liebl, U., Lambry, J. C., Breton, J., Martin, J. L., and Vos, M. H. (1997) Spectral equilibration and primary photochemistry in *Heliobacillus mobilis* at cryogenic temperature, *Biochemistry 36*, 5912−5920.
11. Lin, S., Chiou, H. C., Kleinherenbrink, F. A. M., and Blankenship, R. E. (1994) Time-resolved spectroscopy of energy and electron-transfer processes in the photosynthetic bacterium *Heliobacillus mobilis*, *Biophys. J. 66*, 437−445.
12. Trost, J. T., and Blankenship, R. E. (1989) Isolation of a photoactive photosynthetic reaction center-core antenna complex from *Heliobacillus mobilis*, *Biochemistry 28*, 9898−9904.
13. Brok, M., Vasmel, H., Horikx, J. T. C., and Hoff, A. J. (1986) Electron transport components of *Heliobacterium chlorum* investigated by EPR spectroscopy at 9 and 34 GHz, *FEBS Lett. 194*, 322−326.
14. Muhiuddin, I. P., Rigby, S. E., Evans, M. C., Amesz, J., and Heathcote, P. (1999) ENDOR and special TRIPLE resonance spectroscopy of photoaccumulated semiquinone electron acceptors in the reaction centers of green sulfur bacteria and heliobacteria, *Biochemistry 38*, 7159−7167.
15. Brettel, K., Leibl, W., and Liebl, U. (1998) Electron transfer in the heliobacterial reaction center: Evidence against a quinone-type electron acceptor functioning analogous to A_1 in photosystem I, *Biochim. Biophys. Acta 1363*, 175−181.
16. Kleinherenbrink, F. A., Chiou, H. C., LoBrutto, R., and Blankenship, R. E. (1994) Spectroscopic evidence for the presence of an iron−sulfur center similar to F_X of Photosystem I in *Heliobacillus mobilis*, *Photosynth. Res. 41*, 115−123.

17. Liebl, U., Mockensturm-Wilson, M., Trost, J. T., Brune, D. C., Blankenship, R. E., and Vermaas, W. (1993) Single core polypeptide in the reaction center of the photosynthetic bacterium *Heliobacillus mobilis*: Structural implications and relations to other photosystems, *Proc. Natl. Acad. Sci. U.S.A. 90*, 7124−7128.
18. Nitschke, W., Feiler, U., and Rutherford, A. W. (1990) Photosynthetic reaction center of green sulfur bacteria studied by EPR, *Biochemistry 29*, 3834−3842.
19. Kimble, L. K., Mandelco, L., Woese, C. R., and Madigan, M. T. (1995) *Heliobacterium modesticaldum*, sp-Nov, a thermophilic heliobacterium of hot-springs and volcanic soils, *Arch. Microbiol. 163*, 259−267.
20. Heinnickel, M., Shen, G., Agalarov, R., and Golbeck, J. H. (2005) Resolution and reconstitution of a bound Fe−S protein from the photosynthetic reaction center of *Heliobacterium modesticaldum*, *Biochemistry 44*, 9950−9960.
21. Neerken, S., and Amesz, J. (2001) The antenna reaction center complex of heliobacteria: Composition, energy conversion and electron transfer, *Biochim. Biophys. Acta 1507*, 278−290.
22. Kennedy, M. C., Kent, T. A., Emptage, M., Merkle, H., Beinert, H., and Münck, E. (1984) Evidence for the formation of a linear [3Fe-4S] cluster in partially unfolded aconitase, *J. Biol. Chem. 259*, 14463−14471.
23. Duderstadt, R. E., Brereton, P. S., Adams, M. W., and Johnson, M. K. (1999) A pure S = 3/2 $[Fe_4S_4]^+$ cluster in the A33Y variant of *Pyrococcus furiosus* ferredoxin, *FEBS Lett. 454*, 21−26.
24. Albouy, D., Sturgis, J. N., Feiler, U., Nitschke, W., and Robert, B. (1997) Membrane-associated c-type cytochromes from the green sulfur bacterium *Chlorobium limicola forma thiosulfatophilum*: Purification and characterization of cytochrome c_{553}, *Biochemistry 36*, 1927−1932.
25. Debrunner, P. G. (1989) Mössbauer spectroscopy of iron porphyrins, *Phys. Bioinorg. Chem. Ser. 4*, 137−234.
26. Dwivedi, A., Toscano, W. A., Jr., and Debrunner, P. G. (1979) Mössbauer studies of cytochrome c_{551}. Intrinsic heterogeneity related to g-strain, *Biochim. Biophys. Acta 576*, 502−508.
27. Blankenship, R. E. (2002) *Molecular Mechanisms of Photosynthesis*, Blackwell Science, Ltd., London.
28. Holloway, P. J., Maclean, D. J., and Scott, K. J. (1987) Measurement of cytochrome *f* in thylakoids of higher plants using quantitative gel electrophoresis, *Anal. Biochem. 164*, 31−34.
29. Glerup, J., and Weihe, H. (1991) Magnetic susceptibility and EPR spectra of m-cyano-bis[pentaamminechromium(III)] perchlorate, *Acta Chem. Scand. 45*, 444−448.
30. Glerup, J., and Weihe, H. (1997) Magnetic susceptibility and EPR spectra of (μ-hydroxo)bis[pentaamminechromium(III)] chloride monohydrate, *Inorg. Chem. 36*, 2816−2819.
31. Jacobsen, C. J. H., Pedersen, E., Villadsen, J., and Weihe, H. (1993) ESR characterization of trans-diacidatotetrakis(pyridine)-vanadium and -manganese trans-$V^{II}(py)_4X_2$ and trans-$Mn^{II}(py)_4X_2$ (X = NCS, Cl, Br, I; py = pyridine), *Inorg. Chem. 32*, 1216−1221.
32. Lindahl, P. A., Day, E. P., Kent, T. A., Orme-Johnson, W. H., and Münck, E. (1985) Mössbauer, EPR, and magnetization studies of the *Azotobacter vinelandii* Fe protein. Evidence for a [4Fe-4S]$^{1+}$ cluster with spin S = 3/2, *J. Biol. Chem. 260*, 11160−11173.
33. Yoo, S. J., Angove, H. C., Burgess, B. K., Hendrich, M. P., and Münck, E. (1999) Mössbauer and integer-spin EPR studies and spin-coupling analysis of the [4Fe-4S]^0 cluster of the Fe protein from *Azotobacter vinelandii* nitrogenase, *J. Am. Chem. Soc. 121*, 2534−2545.
34. Mouesca, J.-M., Noodleman, L., Case, D. A., and Lamotte, B. (1995) Spin densities and spin coupling in iron−sulfur clusters: A new analysis of hyperfine coupling constants, *Inorg. Chem. 34*, 4347−4359.
35. Vassiliev, I. R., Antonkine, M. L., and Golbeck, J. H. (2001) Iron−sulfur clusters in type I reaction centers, *Biochim. Biophys. Acta 1507*, 139−160.
36. Zambrano, I. C., Kowal, A. T., Mortenson, L. E., Adams, M. W. W., and Johnson, M. K. (1989) Magnetic circular dichroism and electron paramagnetic resonance studies of hydrogenases I and II from *Clostridium pasteurianum*, *J. Biol. Chem. 264*, 20974−20983.
37. Conover, R. C., Kowal, A. T., Fu, W. G., Park, J. B., Aono, S., Adams, M. W. W., and Johnson, M. K. (1990) Spectroscopic characterization of the novel iron−sulfur cluster in *Pyrococcus furiosus* ferredoxin, *J. Biol. Chem. 265*, 8533−8541.
38. Koehler, B. P., Mukund, S., Conover, R. C., Dhawan, I. K., Roy, R., Adams, M. W. W., and Johnson, M. K. (1996) Spectroscopic characterization of the tungsten and iron centers in aldehyde ferredoxin oxidoreductases from two hyperthermophilic archaea, *J. Am. Chem. Soc. 118*, 12391−12405.
39. Georgiadis, M., Komiya, H., Chakrabarti, P., Woo, D., Kornuc, J., and Rees, D. (1992) Crystallographic structure of the nitrogenase iron protein from *Azotobacter vinelandii*, *Science 257*, 1653−1659.
40. Duderstadt, R. E., Staples, C. R., Brereton, P. S., Adams, M. W. W., and Johnson, M. K. (1999) Effects of mutations in aspartate 14 on the spectroscopic properties of the $[Fe_3S_4]^{+,0}$ clusters in *Pyrococcus furiosus* ferredoxin, *Biochemistry 38*, 10585−10593.
41. Nuijs, A. M., van Dorssen, R. J., Duysens, L. N. M., and Amesz, J. (1985) Excited states and primary photochemical reactions in the photosynthetic bacterium *Heliobacerium chlorum*, *Proc. Natl. Acad. Sci. U.S.A. 82*, 6865−6868.
42. Kobayashi, M., van de Meent, E. J., Erkelens, C., Amesz, J., Ikegami, I., and Watanage, T. (1991) Bacteriochlorophyll *g* epimer as a possible reaction center component of heliobacteria, *Biochim. Biophys. Acta 1057*, 89−96.

BI060031S